

Solar Prominences, Solar Flares and Coronal Mass Ejections

A Solar Physics Report

Péter I. Pápics^{1,2}

¹ Eötvös Loránd University, Department of Astronomy (Hungary)

² Katholieke Universiteit Leuven, Institute of Astronomy (Belgium)

Task received 6 December 2007 / Deadline 21 December 2007

ABSTRACT

In this report, I give a detailed description of selected activity phenomena on the Sun – Solar Prominences, and in connection with them the Solar Flares and the Coronal Mass Ejections (CMEs). I discuss the basic facts about these phenomena (focusing on prominences); the history of observations (from the beginning to the most recent observations of latest space probes), the classification (morphology) and the most important observational characteristics. Later, I explain their origin, the role of thermal instability, some of the corresponding (MHD) models and simulations, etc. Finally I give a short summary about the relation between prominences and solar flares (and CMEs).

Key words. Sun: prominences – Sun: flares – Sun: coronal mass ejections (CMEs) – Sun: magnetic fields – MHD

1. Introduction

The Sun, and the active phenomena of the Sun are a real test field for plasma physics. Understanding the nature of our star is not only important for the scientists, but through better space weather predictions it makes a significant impact on our everyday life in our technology-dependent life in the 21st century.

Large amplitude fluctuations in the Solar wind mainly due to flares and coronal mass ejections (CMEs) are critical to be predicted (or at least observed in time), because the high-energy particles and the magnetic field fluctuations are really dangerous for high precision instruments, such as telecommunication satellites, power transmission networks, space stations, but also for people on board commercial airplanes flying on high latitude (polar) routes. During the latest Solar maximum several huge blackouts showed the force of the active Sun, which can not be ignored by us.

These components of the space weather are all originate in the Sun – a plasma sphere with a radius of ≈ 700000 km, with a strong and not so simple magnetic field driven by the Solar Dynamo. As the quasi neutral gas of ionised and neutral particles interacts with the magnetic field we need magnetohydrodynamics (MHD) to describe the motions in the atmosphere of the Sun (see Fig. 1), where the most important and easily observable activity features are located.

2. Activity phenomena

The Sun is probably among the first celestial bodies which were observed in the prehistoric times. There are no (or only very few) as shocking displays on the sky as a total Solar eclipse, when one component of the Solar atmosphere is already clearly visible to the naked eye – the *Corona*. But we do not have to go this far, there are much natural and more simple causes why the Sun become one of the most important subject of observations. The Sun is the source of warmth, the source of energy so the

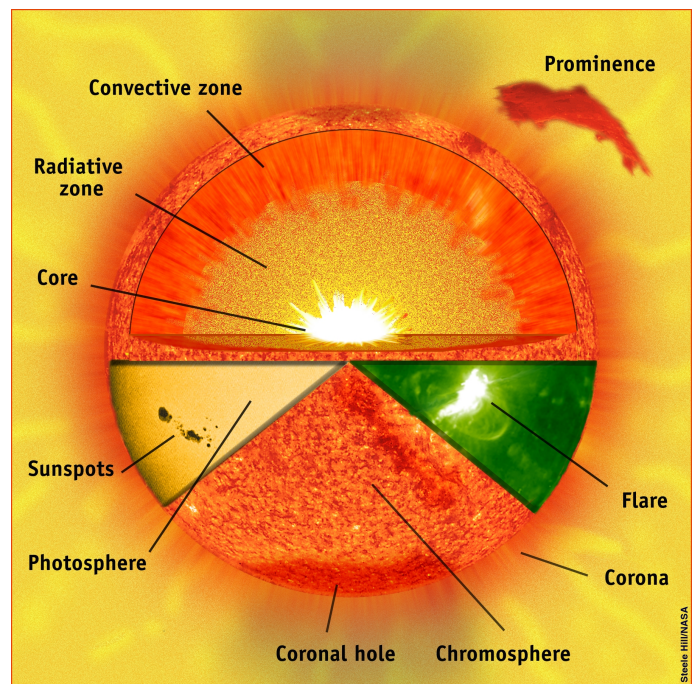


Fig. 1. A basic overview of the parts of the Sun. The three major interior zones are the core (the innermost part of the Sun where energy is generated by nuclear reactions), the radiative zone (where energy travels outward by radiation through about 70% of the Sun), and the convection zone (in which convection currents circulate the Sun's energy to the surface). The flare, sunspots and photosphere, chromosphere, and the prominence are all clipped from actual SOHO images of the Sun.

source of Life – and this was very early understood by the humans through the periodic change of seasons connected with the height of the midday Sun on the sky. Later the growing importance of calendars strengthened the role of the Sun in the every-

day life. The impact on the early societies is well represented by the wide range of Sun Gods in the cultures of the first civilisations.

The second, and (not counting other sporadic observations) the last features observed on the Sun until the 19th century are the *sunspots*. The first observations were made probably through mist or clouds in the morning or at the evening. The sign of the Sun (☉) originates in the ancient Egypt, which could also refer to the early observations. The first written documentation of a sunspot was made in the 4th century BC by a student of Aristotle. Strange coincidence, that the ancient Greeks, and other Europeans after them, were highly influenced by the teachings of Aristotle, who held that the Sun and the heavens were ideal, an embodiment of unblemished perfection. That's why none of them were really interested in the Sun in the following centuries.

But after the invention of the telescope, suddenly everything had changed. Galileo Galilei turned his telescope to the Sun, and discovered sunspots – now without doubts. But their origin remained a mystery for centuries. The Solar Cycle was only recognised in 1843 by Samuel Heinrich Schwabe, who after 17 years of diligent observations of the Sun noticed a periodic variation (with a period of ≈ 11 years) in the average number of sunspots seen from year to year on the Solar disk. Its basic characteristics were described by Gustav Spörer, Richard Carrington and George Ellery Hale.

As the other phenomena of the Sun are strongly connected with the Solar cycle (they are more likely to happen around the maximum), let's have a look at on the main laws described by the scientists mentioned above.

- The polarity orientations of the bipolar active regions are found to obey the well-known Hale polarity law (Hale et al. 1919; Hale & Nicholson 1925) outlined as follows. The line connecting the centers of the two magnetic polarity areas of each bipolar active region is usually nearly east-west oriented. Within each 11-year Solar cycle, the leading polarities (leading in the direction of Solar rotation) of nearly all active regions on one hemisphere are the same and are opposite to those on the other hemisphere, and the polarity order reverses on both hemispheres with the beginning of the next cycle. The magnetic fields at the Solar north and south poles are also found to reverse sign every 11 years near sunspot maximum (i.e. near the middle of a Solar cycle). Therefore, the complete magnetic cycle, which corresponds to the interval between successive appearances at mid-latitudes of active regions with the same polarity arrangement, is in fact 22 years.
- Spörer's law: The active regions are roughly confined into two latitudinal belts which are located nearly symmetrically on the two hemispheres. Over the course of each 11-year Solar cycle, the active region belts march progressively from mid-latitude of roughly 35° to the equator on both hemispheres (Maunder 1922).

2.1. Prominences

2.1.1. History

Prominences were first seen probably during total Solar eclipses, but only some sporadic observations were made before the 19th century, describing them for example as “burning holes” (Ludovico Antonio Muratori 1239) or “red flames” (Vassenius 1733). In 1842 during a total eclipse visible from South Europe (on the 8th of July) many observers recognised these features –

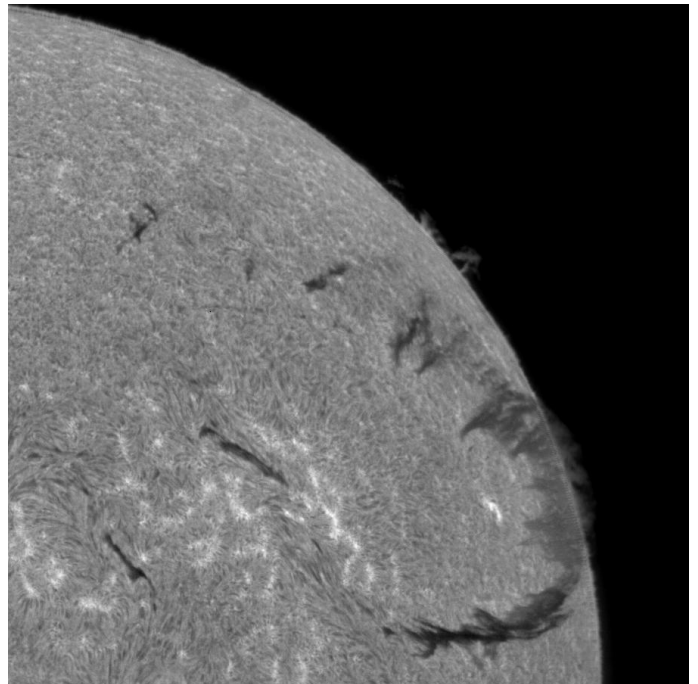


Fig. 2. $H\alpha$ image of the Sun taken on 20 January 2004 showing several filaments and protuberances – filaments “hanging” above the rim of the Solar disk. Image credit: Big Bear Solar Observatory.

so this was the discovery for science. The first spectra were made during an eclipse in 1868, and that made clear, that prominences are gas clouds (Pierre Janssen and Joseph Norman Lockyer independently observed bright emission lines of a previously unknown element later named Helium). In the 1890s spectroheliograph observations led to the discovery of filaments (which are prominences seen on the disc of the Sun, see Fig. 2 and Fig 3). First polarimetric observations of prominences were made by Zirin & Severny (1961).

2.1.2. Characteristics

The first classification was made by Angelo Secchi who distinguished between quiescent (see Fig. 3) and eruptive prominences in the 1870s. Quiescent prominences are (from the Introduction of Galsgaard & Longbottom (1999)) one of the largest “individual” magnetic features on the Sun. They form on the timescale of a day, and typically remain “unchanged” for up to a month (or even six months – but only larger-scale structures remain fixed while the fine structure changes rather rapidly) and often end their existence through an eruption as part of a coronal mass ejection (CME, see Section 4 from more info). Prominences are located in the Solar corona and consist of plasma that has parameters comparable to that of the chromosphere – they are cold and dense compared to the surrounding corona.

The basic parameters of quiescent prominences are the following (from the Lecture Notes of K. Petrovay). Quiescent prominences may form A) in active regions (but it is the less common), B) between two active regions or C) over polar crown neutral line, near an expanding AR. They are supported against gravity by magnetic forces. They have a length of 60 to 600 Mm, a height (above the chromosphere) ranging from 15 to 100 Mm, a width of 5 to 15 Mm, a temperature of 4300 to 8500 K, an average electron density of $10^{10} - 10^{11} \text{ cm}^{-3}$, a pressure of $0.1 - 1 \text{ dyn/cm}^2$, a magnetic field strength of 4 to 20 G (Bommier

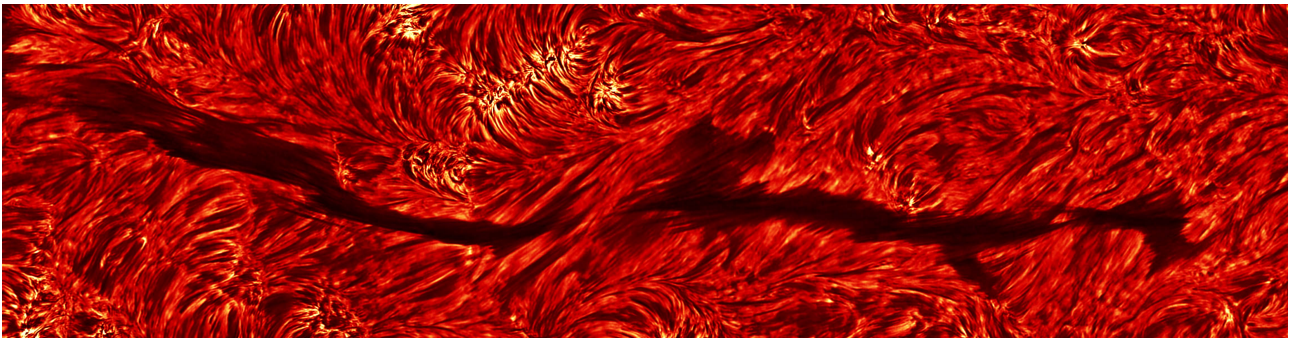


Fig. 3. Dutch Open Telescope (DOT) picture of the Sun showing a filament, or in other words a quiescent prominence. Image mosaic covering the full length of a filament, taken in H α on 6 October 2004.

et al. 1994; Leroy et al. 1983; Athay et al. 1983) and an ionization fraction of $\approx 0.2-0.9$ (meaning the freezing in is OK). Their internal motions have a speed below 10 km/s.

There are several classification schemes for prominences, I will present a short selection of them (from the Lecture Notes of K. Petrovay). Prominence fine-structure morphology manifests itself rather differently in case of the limb observations and in case of disk filaments. Moreover, one has to clearly distinguish between typical quiescent and active-region prominences or filaments. Generally speaking, a prominence seen on the limb has appeared before or will appear later as a filament on the disk. In case of quiescent prominences larger-scale structures remain fixed while the fine structure changes rather rapidly (Heinzl 2007). Prominences can be connected with active regions, or they can just “float” above the quiet chromosphere. The first classification scheme is shown in Fig. 4. If a quiescent prominence

By location		By dynamics
Quiet Sun / Active Region (AR)	Combined types	Steady / fast varying
Quiescent prominences	or Quiescent filaments	} Filaments
Plage (or AR) prominences	{ Plage (or AR) filaments	
	Active prominences	Active prominences

Fig. 4. Basic classification scheme for Solar Prominences

starts to rise with increasing speed, we talk about an eruptive protuberance, also known as a *disparition brusque* (DB). Later this kind of prominence can leave the Sun through a CME. So after the introduction of eruptive prominences, we can use the alternate classification scheme which is shown in Fig. 5. Of course

	Steady shape	Varying shape
On quiet Sun:	Quiescent filaments	Eruptive prominences (DBs)
In active regions	Plage filaments	Active prominences

Fig. 5. Alternate classification scheme for Solar Prominences

there are further intermediate cases, as some quiescent prominences end in a sunspot – from their end, matter flows into the spot.

In the case of quiescent prominences, one can distinguish between polar (or polar crown) filaments, and low-latitude (or sunspot, or sunspot belt) filaments. The formers are the largest, longest lived, and quietest prominences, while the latter can

end in sunspots. There are also the so-called plage filaments – these are smaller, shorter lived (< 1 day), their magnetic field is stronger (20 – 70 G), and there is a flow along the filament with $v < 60$ km/s. For more details on the fine structure (and the observations of Solar Prominences), see Subsection 2.1.3.

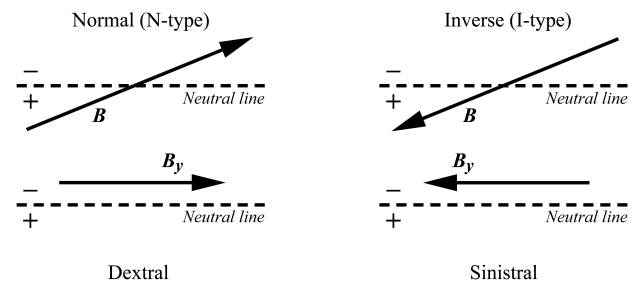


Fig. 6. Magnetic types (at the top) and Chirality types (at the bottom) of Solar prominences.

I am not going into details here, but based on the magnetic field line configurations in and around the prominence one can distinguish between Normal (N-type – they are all located below 30 Mm) and Inverse (I-type – more common among polar filaments) prominences (see Fig. 6 and the corresponding models in Section 3). Based on the orientation of the magnetic field component parallel to the neutral line, we are talking about Chirality types (see Fig. 6) – dextral prominences dominate on the Northern hemisphere, sinistrals in the Southern.

A quiescent prominence can be activated by external disturbances (e.g. magnetic reconnection near the filament – so these are really connected with other phenomena described in this section). In an active prominence the internal motions are increased ($v = 30 - 50$ km/s, occasionally much more) and so the temperature is for some hours. At the end of the active state, a filament returns to its normal state or erupts (\Rightarrow Eruptive prominence – see Fig. 7). There are several types of active prominences: Surge, Spray, Fast ejection, Loop prominences (flaring arches, postflare loops), Coronal rain and Coronal cloud. Surges are columns (vertical, or slightly curved), they shot up, than fall back in the same way at the same place, having $v \approx 100 - 200$ km/s, a maximum height of $h \approx 100 - 200$ Mm and a timescale $\tau \approx 10 - 20$ minutes. Spray: blob shot up, fragments, then often leaves the Sun. $v \approx 500 - 1200$ km/s. They typically result from DB of plage filament. Fast ejection: compact blob shot up from a flare, $v \approx 1000$ km/s. Flaring arches: plasma shot into magnetic loop (often by flare) and flows along it. Postflare loops: matter condenses at top of flare loop, then flows down in both

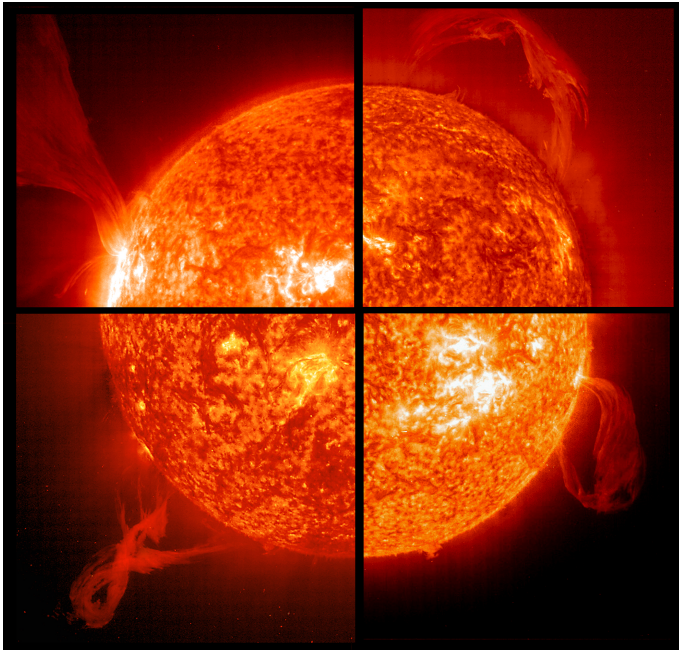


Fig. 7. SOHO EIT image of eruptive prominences in the 304 Angström spectral line. Going clockwise from the upper left, the images are from: 15 May 2001, 28 March 2000, 18 January 2000, and 2 February 2001.

legs. A Coronal rain is similar to a postflare loop, but intermittent. Coronal cloud: irregular plasma blob floating in corona for a while, with matter streaming out of it along field lines.

2.1.3. Observations

Despite the fact that prominences have been observed for decades, they are still not well understood. It is not known how they form and provide support against gravity for the enhanced density in the corona. The force balance in the corona is controlled by the magnetic field, and static two-dimensional models have addressed the support problem using different magnetic topologies (Kippenhahn & Schlüter 1957; Kuperus & Raadu 1974) – as it is explained in Section 3. While these provide some information about the possible magnetic topology in the quiescent phase, they cannot explain how prominences are formed, nor do they provide an explanation for the observed three-dimensional structures or the course for the final eruption. Before the creation of models, detailed observations are needed to study the fine structure and the whole life of a prominence.

Prominences can be observed in a wide wavelength range corresponding to the temperature of their plasma and of the surrounding volume. Limb-prominences can be seen also by amateur astronomers in visible wavelengths using a coronagraph, or at total Solar eclipses, while filaments are easy to observe through a $H\alpha$ telescope. Of course the most valuable data is coming from high-resolution ground-based telescopes and space instruments.

When observed in $H\alpha$, quiescent prominences appear on the Solar disk as long, thin absorption features over a line of magnetic-polarity inversion on the photosphere (see Fig. 3). When viewed at the Solar limb in its own $H\alpha$ emission, prominences are showing a variety of shapes. Now following the article of Heinzel (2007) I will present some instruments, mentioning some recent results obtained with them.

Our information about the fine structure morphology and dynamics comes from currently available high-resolution ground-based observations mostly made in the $H\alpha$ line. With the instruments like the new SST (Swedish 1-m Solar Telescope) or DOT (Dutch Open Telescope), one can see fine structures down to the resolution limit ($0.15''$ for SST or around 100 km). Homogeneous time series are now expected with a similar spatial resolution from the Solar Optical Telescope (SOT) onboard the Hinode satellite.

A large variety of fine structures and their dynamics is also seen on TRACE movies, although the spatial resolution is lower, around $1''$. These images are usually taken with a 171 or 195 Angström filter where the hot coronal structures appear simultaneously with cool ones. (The Extreme ultraviolet Imaging Telescope – EIT – on board the SOHO probe also observes in this wavelength range, but with a much lower resolution.) Cool prominences or filaments are dark against the bright background which is due to the absorption of the background coronal radiation emitted in these lines by the hydrogen and helium resonance continua (see cartoon in Rutten (1999)) and partially due to lack of emissivity of the TRACE lines within a volume occupied by cool prominence plasmas. At 171 or 195 Angström, the HeI and HeII absorption dominates over the HI and it was shown theoretically that this opacity is quite comparable to that of the $H\alpha$ line (Anzer & Heinzel 2005).

Continuous (affected only by the impact of local weather) $H\alpha$ observations are made in the Big Bear Solar Observatory (BBSO), with a resolution high enough to show many vertically oriented threads of the cool plasma which are a few hundred kilometres wide (Low & Petrie 2005) in quiescent prominences. On a larger scale, one can identify a few vertical plasma sheets which, using a lower spatial resolution, would appear as more-or-less homogeneous slabs with the thickness typically smaller compared to the other two spatial dimensions. Such a kind of low resolution images led modelers to use a vertical 1D slab approximation to a real prominence geometry which completely neglected the fine structure.

On the disk, the high-resolution $H\alpha$ images or movies show fine-structure fibrils of different lengths, the thinnest visible down to the resolution limit of SST or DOT. Very thin dark fibrils visible along the spine of a quiescent filament are rather short and inclined to the filament axis due to the shear of the magnetic field lines (see Fig. 3).

Today one can study the fine-structure dynamics and prominence evolution on prominence/filament movies taken by TRACE in the 195 Angström line or on high-resolution $H\alpha$ images or movies. Within the disk filaments, individual fibrils move sideways with velocities up to 3 km s^{-1} which seems to be consistent with limb observations of Zirker & Koutchmy (1990, 1991). For more see the paper of Heinzel (2007).

At last, it is important to note that both quiescent and active-region prominences, if large enough to be observed on the disk in radio waves, show a region of depressed radio emissions attributed to a low-density cavity around the filament.

2.2. Flares

Solar Flares are violent “explosions”, observed as sudden brightenings in the Solar atmosphere above active regions (sunspot groups). They take place in the chromosphere and the corona, but the strongest ones can heat up even the photosphere (producing a flare visible even in white light). The first Solar flare was observed in 1859 by Richard Carrington, who was drawing sunspots, when he suddenly noticed two bright spots in one

of the sunspot groups. They brightened and faded in just ten minutes. Carrington already noticed that this phenomena was followed by the appearance of northern lights on the following night. These white-flares are very rare, less than a hundred of them were observed in the last century. In the short-wavelength range (UV and X-ray) the brightening is even more bigger. During a flare, the total ultraviolet radiation of the Sun rises with a significant factor, while the level of sum X-ray radiation from the Sun can grow with orders of magnitudes.

Contrary to the case of the white-flares, “normal” ones are quite common. After the start of continuous observations in $H\alpha$, it turned out, that around Solar maximum there could be as many as 30 – 40 or even a hundred flares on an average day. In Solar minimum, there can be weeks without flares (e.g. October 2007). So we can see that $H\alpha$ flares are more common, but X-ray flares are even more so. This shows that the energy is liberated in the corona, and the bigger the flare, the deeper layer is affected by it. So flares are powered by the sudden (timescales of minutes to tens of minutes) release of magnetic energy stored in the corona. The energy release is $\leq 10^{33}$ erg while the temperature is $\leq 7 \times 10^7$ K – what is higher than the temperature in the center of the Sun!

Beside the heating of the plasma, flares accelerate electrons, protons and heavier ions to near the speed of light. They produce electromagnetic radiation across the electromagnetic spectrum at all wavelengths from long-wave radio to the shortest wavelength gamma rays. X-rays and UV radiation emitted by Solar flares can affect Earth’s ionosphere and disrupt long-range radio communications. Direct radio emission at decimetric wavelengths may disturb operation of radars and other devices operating at these frequencies. Solar flares and associated Coronal Mass Ejections (CMEs) strongly influence our local space weather. They produce streams of highly energetic particles in the Solar wind and the Earth’s magnetosphere that can present radiation hazards to spacecraft and astronauts. The soft X-ray flux of X class flares increases the ionisation of the upper atmosphere, which can interfere with short-wave radio communication, and can increase the drag on low orbiting satellites, leading to orbital decay. Energetic particles in the magnetosphere contribute to the Aurora Borealis and Aurora Australis.

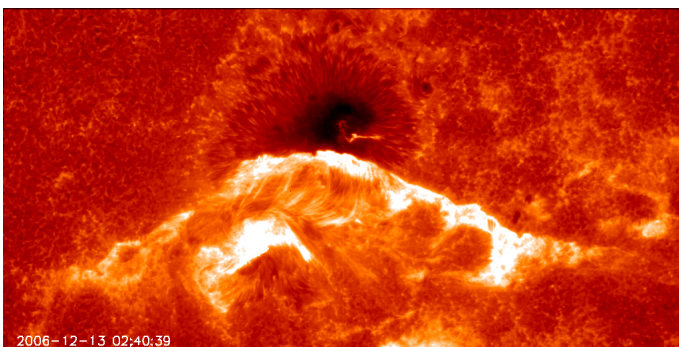


Fig. 8. Hinode (Solar-B) image of a Solar flare. SOT image in CaII H spectral line shows separating flare ribbon in the chromosphere. Finestructure of flare loops are also noticed. The field of view is $216''$ by $108''$ corresponding to 1.6×10^5 km by 7.9×10^4 km on the Sun.

One possible classification of Solar flares is based on morphology. One can distinguish between Two-ribbon flares (generally these are the big ones, always associated with erupting filaments) and Compact flares. The two-ribbon flares are showing two parallel bright ribbons separating in time (see Fig. 8).

Another classification scheme is based on the energy of the flare. Solar flares are classified as A, B, C, M or X according to the peak flux (in watts per square meter, W/m^2) of 100 to 800 picometer X-rays near Earth, as measured on the GOES spacecraft. Each class has a peak flux ten times greater than the preceding one, with X class flares having a peak flux higher than $10^{-4} W/m^2$. Within a class there is a linear scale from 1 to 9, so an X2 flare is twice as powerful as an X1 flare, and is four times more powerful than an M5 flare. The largest GOES flare was an event on 4 November 2003, originally classified as X28, but it turned out that the detectors were saturated at the peak of the flare, and based on the influence of the event on the Earth’s atmosphere it was between X40 and X45.

In X-ray images we can see postflare loops, from which the old ones are cool, but new, hot loops keep forming above them. It shows, that a flare involves change in magnetic structure, so it is connected with magnetic reconnection. The simplest model includes an X-point reconnection, which develops into growing current sheet, and accelerate particles in two jets – observational evidence: upper coronal X sources. Particles emitted downwards cause observed flare emission. For more, see Section 3.

How does the energy propagate (from the Sun to the Earth)? There are different arrival times for different particles. 1) Proton flares: flares accompanied by 1 – 50 GeV proton shower. This “Solar cosmic ray-shower” arrives in 10 – 20 minutes and lasts 10 – 20 minutes. 2) Polar Cap Absorption (PCA): Ionospheric increase at high latitudes caused by 1–600 MeV electrons. They arrive in 1 – 2 hours. 3) Geomagnetic activity related to flares: magnetic storms, aurorae. Due to 1 – 100 keV electrons. They arrive in 1 – 2 days. Flares are accompanied by radio bursts.

2.3. Coronal Mass Ejections

Coronal mass ejections are large eruptions of mass and magnetic field from the Sun. More generally, they are Coronal transients: short-lived changes in coronal structure – outward moving new bright features in K corona. Although only discovered in the early 1970s (the first detection of a CME was made on 14 December 1971 by R. Tousey using the 7th Orbiting Solar Observatory (OSO-7), see also SKYLAB results from MacQueen et al. (1974)), the effects of CMEs have been seen indirectly at Earth for many thousands of years, mainly because the impact of a CME on the Earth’s magnetosphere can generate an aurora. When the ejecta reaches the Earth as an ICME (Interplanetary CME), it may disrupt the Earth’s magnetosphere, compressing it on the dayside and extending the nightside tail. When the magnetosphere reconnects on the nightside, it creates trillions of watts of power which is directed back towards the Earth’s upper atmosphere. This process can cause particularly strong aurora also known as the Northern Lights, or Aurora Borealis (in the Northern Hemisphere), and the Southern Lights, or Aurora Australis (in the Southern Hemisphere). CME events, along with Solar flares, can disrupt radio transmissions, cause power outages (blackouts), and cause damage to satellites and electrical transmission lines.

The morphology of many CMEs observed in this way consists of a threepart structure (Plunkett et al. 2000) which is clearly visible on the left image of Fig. 9: a bright leading edge, dark cavity and a bright core or kernel (Illing & Hundhausen 1986). The bright core is often identified as cool, dense prominence material – a remnant of an eruptive prominence (Crifo et al. 1983; Sime et al. 1984; Low 1994), although it is difficult to prove such an association from white-light coronal observations alone. The pre-CME coronal structure is frequently identified as

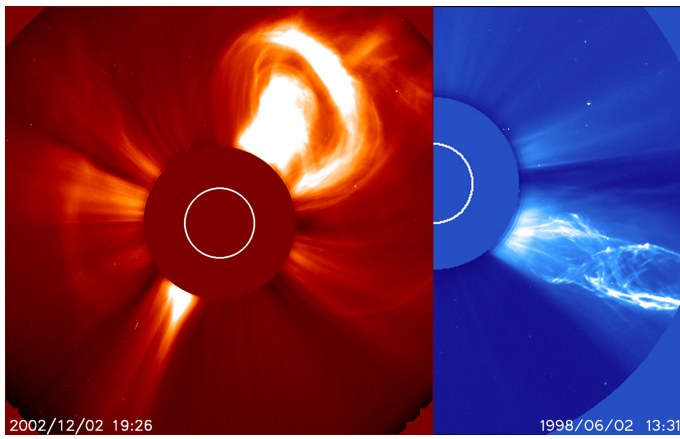


Fig. 9. Two images from the Solar and Heliospheric Observatory (SOHO) taken with the LASCO C2 coronagraph. At the left: a large coronal mass ejection (CME) blasting off into space on 2 December 2002. It presents the classic shape of a CME: a large bulbous front with a second, more compact, inner core of hot plasma (the erupting prominence) – see text for more detailed explanation. At the right: a twisting, helical-shaped CME spins off from the Sun. This particular CME and erupting prominence is somewhat unusual in that the width of the blast is relatively narrow and the strands of plasma are twisting. The white circle represents the size and position of the Sun.

a helmet streamer with a high-density dome, a low-density cavity and an embedded prominence at the base of the cavity. It should be noted, however, that many CMEs are missing one of these elements, or even all three.

Most CMEs originate from active regions. These regions have closed magnetic field lines, where the magnetic field strength is large enough to allow the containment of the plasma; the CME must open these field lines at least partially to escape from the sun. However, CMEs can also be initiated in quiet sun regions (although in many cases the quiet region was recently active). During Solar minimum, CMEs form primarily in the coronal streamer belt near the Solar magnetic equator. During Solar maximum, CMEs originate from active regions whose latitudinal distribution is more homogenous.

Coronal Mass Ejections range in speed from about 20 km s^{-1} to $2,700 \text{ km s}^{-1}$ with an average speed (based on SOHO/LASCO measurements between 1996 and 2003) of 489 km s^{-1} . The average mass based on coronagraph images is $1.6 \times 10^{15} \text{ g}$. Due to the two-dimensional nature of the coronagraph measurements, these values are lower limits. The frequency of ejections depends on the phase of the Solar cycle: from about one every other day near Solar minimum to 5-6 per day near Solar maximum. These values are also lower limits because CMEs propagating away from the Earth (“backside CMEs”) can usually not be detected by coronagraphs.

The Large Angle and Spectrometric Coronagraph Experiment (LASCO) instrument on board of SOHO is monitoring the CMEs continuously from 1995. The most recent instruments are on board the NASA STEREO mission, which was launched in 2006. The mission objective is to understand the 3D nature of CMEs, their initiation and propagation. It consist of two identically instrumented spacecraft on a heliocentric orbit, one leading Earth and one trailing. The instrument complement consists of optical and radio remote sensors as well as in-situ measurements of energetic particles and Solar wind composition.

3. Modeling

May be the most effective way of testing theories is modeling. Models based on various physical equations (e.g. MHD models with boundary conditions, jump conditions and starting values), observed quantities, and of course assumptions, are very efficient in showing are we already right now, or there is still a long way to go before the full understanding of the nature of magnetohydrodynamical processes in the atmosphere of our Sun. Of course, there is still a long way to go, but the scientific community is getting closer and closer with every try and every publication. In the following subsections I will give an overview about some of the basic and most widely accepted and used models for different Solar phenomena through some literature study.

3.1. Prominences

Although the fine structure was known, the prominences have been modeled for decades as a whole, using simplified one-dimensional (1D) slab models. The two basic topological models – showing the magnetohydrostatic (MHS) structure – of prominences are the Kippenhahn-Schlüter model (1957 – upward Lorentz-forces supporting the prominence against gravity) and the Kuperus-Raadu model (1974), which are shown in the a) and c) part of Fig. 10 (but not with a current-sheet prominence as it was originally proposed in case of the K-R type). Coronal magnetic field measurements have revealed very early these two basic configurations for the coronal field around a prominence. In the former, the photosphere polarity beneath the prominence implies a magnetic field pointing in the same direction as the magnetic field threading across the prominence. In the latter, these two magnetic fields point in opposite directions – the prominence is detached from the photosphere. In both configurations, the magnetic field generally threads across the prominence at a shallow angle of about 20° to the long (horizontal) prominence axis. The strong axial component of the magnetic field gives rise to the often observed helical structures in erupting prominences (see the right hand side image of Fig. 9). In both types the magnetic tension force is supporting the prominence material against gravity.

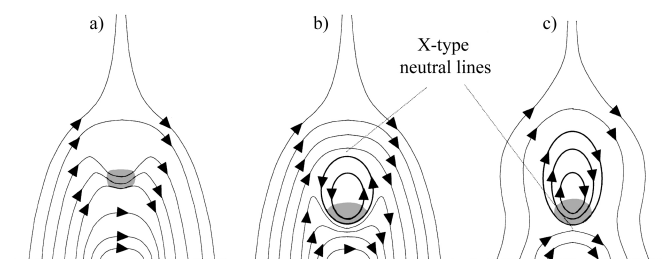


Fig. 10. Schematic diagrams showing the magnetic topologies of three types of prominence support models; the prominences are shown by shaded areas. Figure from Gilbert et al. (2000). From the left to the right: a) Normal Polarity Dip Model (N-type prominences – see Kippenhahn & Schlüter (1957)), b) Normal Polarity Flux Rope Model and c) Inverse Polarity Flux Rope Model (I-type prominence – see Kuperus & Raadu (1974)).

Before the presentation of some selected models, I will say something about the role of thermal instability. Now it is well established, that prominences are formed by condensation of coronal plasma due to thermal instability, what was shown by Field (1965). It is shown there that, under a wide range of conditions,

thermal equilibrium is unstable and can result in the formation of condensations of higher density and lower temperature than are found in the surrounding medium. In the Solar corona the radiative loss increases with decreasing temperature in some temperature range (Cox & Tucker 1969) and is proportional to density squared. Thus if we have a perturbed plasma, which is dense and cool enough to overcome adiabatic and nonadiabatic heat flows, this perturbation can grow until a new equilibrium is met where the radiative loss decreases with decreasing temperature. The calculations there in Section VII/c shown that gas pressure forces alone can lead to the formation, through thermal instability, of quiescent prominences which are similar to those observed in respect to density, dimensions, shape and time scale. It still appeared necessary to assume compression by magnetic forces to account for the short time scales of active prominences, however.

One of the most accepted models was proposed by Pikel’Ner (1971) saying the N-type (K-S type) quiescent prominence is a condensation in or above a sheared arcade, aided by a siphon flow. For stable equilibrium, prominences must be supported with magnetic lines of force leaning upon the photosphere and concave in their tops – however the general structure may be more complicated. The gas of the corona, distributed along the magnetic lines tube, cannot keep balance, it should flow down the pit, condense there and fall down into the cromosphere in some places. The prominence, therefore, originates in the matter of the cromosphere which is situated at the other ends of magnetic lines and flows through the corona under the effect of a syphon-type mechanism.

The model of Choe & Lee (1992) favours this view of material supply from below, but not as an assumption, but as a result of the simulation. They used a numerical 2.5D MHD code to investigate the prominence formation in a magnetic arcade by photospheric shearing motions. In the code they used resistive, viscous MHD equations with the gravitational force, radiative cooling, thermal conduction and a simple coronal heating also included (see the article for details on the equations, normalisation, used radiation loss function, initial and boundary conditions). They adopted a Cartesian geometry ignoring the curvature of the Solar surface. They ignored the dependence of physical variables on the coordinate along the prominence axis (the z -coordinate, while the vertical axis is designated by y). I think that there is not enough space in this report to discuss every detail, but I would like to mention, that the photosphere and cromosphere are collapsed onto the bottom boundary and the corona is assumed to be initially isothermal and in a static equilibrium resulting in a stratified density and pressure profile. They found that a footpoint shear induces an expansion of the magnetic arcade and cooling of plasma in it. Simultaneously the denser material from the lower part of the arcade is pulled up by the expanding field lines. A local enhancement of radiative cooling is thus effected, which leads to the onset of thermal instability and the condensation of coronal plasma. The condensed material grows vertically to form a sheet-like structure making dips on field-lines, leading to the formation of the K-S type prominence. The mass of the prominence is found to be supplied not only by the condensation, but also by the siphon-type upflows. The upward growth of the vertical sheet-structure is saturated at a certain stage and the newly condensed material is found to slide down from above the prominence along magnetic field lines. This drainage of material leads to the formation of arch-shaped cavity of low density and low pressure around the prominence, which is found to be not in a static equilibrium but in a dynamic interaction with its environment. Another interesting

current-sheet model is presented for both N and I-type prominences by Malherbe & Priest (1983).

A model of I-type prominences lying in a helical flux tube was presented by Pneuman (1983), which contains certain aspects of three different theories (those in which the Lorentz forces support the prominence against gravity, those invoking the confinement of current sheet models and the helical models), but, also, some important differences. I am not going into details here but the basic idea is shown in Fig. 11 and described in the caption of the figure.

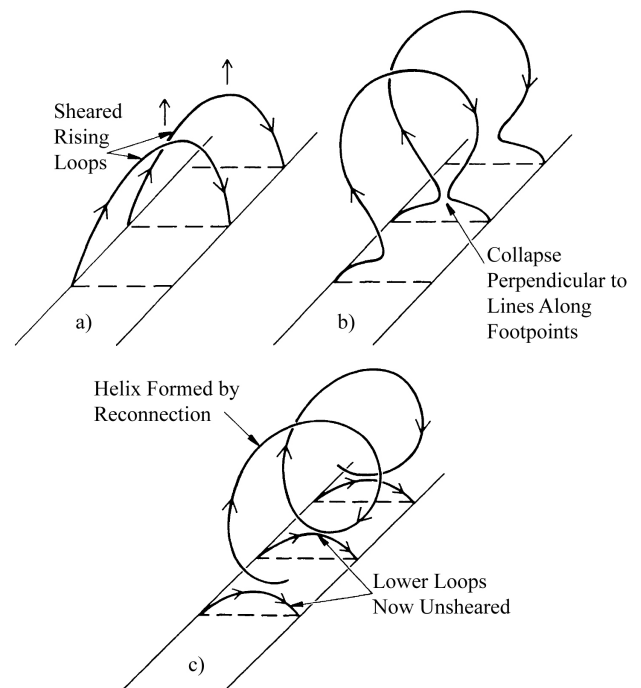


Fig. 11. Schematics showing how a rising, sheared bipolar region might collapse inward producing isolated helices above the neutral line formed and an unsheared new bipolar region below: a) simple rising, sheared bipolar loops; b) inward collapse perpendicular to lines connecting the footprints (shown dashed); and c) reconnection producing helices above neutral line and new, unsheared bipolar region below. Continuing reconnection would actually produce many helices, each nested inside the other. The prominence (not shown) is then formed in the bottom central part of the helices by condensation and downflow.

An alternate theory is the twisted flux tube model proposed by Priest, Hood, & Anzer (1989). It is proposed that a Solar prominence consists of cool plasma supported in a large-scale curved and twisted magnetic flux tube (see Fig. 12). As long as the flux tube is untwisted, its curvature is concave toward the Solar surface, and so it cannot support dense plasma against gravity. However, when it is twisted sufficiently (by Coriolis forces), individual field lines may acquire a convex curvature near their summits and so provide support. Cool plasma then naturally tends to accumulate in such field line dips either by injection from below or by thermal condensation. As the tube twisted up further or reconnection takes place below the prominence, one finds a transition from normal to inverse polarity. When the flux tube becomes too long or is twisted too much, it loses stability and its true magnetic geometry as an erupting prominence is revealed more clearly. Twisting motions of various kinds have

been well observed in prominences. The presented model is essentially 3D. See details in the article.

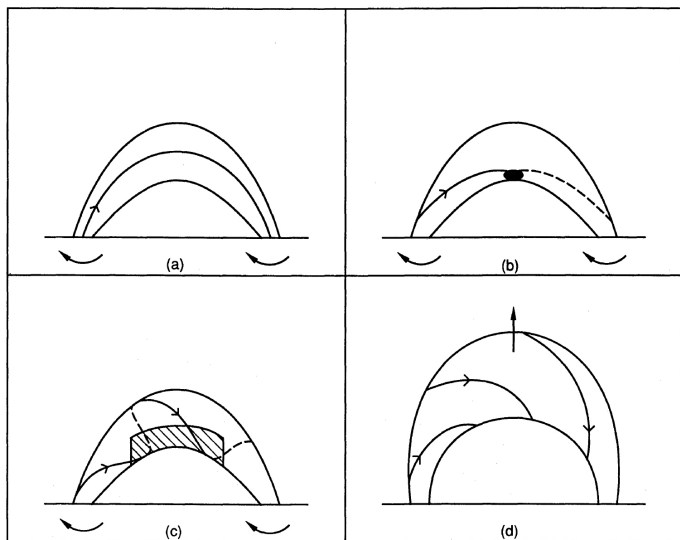


Fig. 12. The evolution of a large flux tube as its twist increases. (a) No twist. (b) Critical twist for prominence formation to start at the tube summit. (c) Larger twist, with the prominence extending along the length where curvature is favourable for support. (d) Such a large twist that the prominence erupts.

3.2. Flares

I just mention here two models, a circuit model from Martens & Kuin (1989) for two-ribbon flares (tightly connected with filament eruptions – see Fig. 2 in their article) and a reconnection-plasmoid ejection model for compact loop flares by Shibata et al. (1995); Shibata (1996). Martens & Kuin derived a model which reproduces the slow energy build up and eruption of the filament, and the energy dissipation in a current sheet at the top of post-flare loops during a two-ribbon flare. In this model, the free magnetic energy is concentrated in a current through the filament, another current in the underlying current sheet, and a surface return currents. The magnetic field configuration generated by these currents and general photospheric background field, has a topology similar to the observed ones. They consider two circuits, that of the filament and its return current, and that of the current sheet and its return current (see Fig. 5. in their article). These circuits are inductively coupled and free energy stored in the filament in the pre-flare phase is found to be transferred to the sheet during the impulsive phase, and rapidly dissipated there. In the solutions they were able to distinguish between 4 phases: (1) a slow energy build up (2 days, filament evolves quasi-statically), (2) metastable state (3 hours, during this the filament is susceptible to flare triggers, and the current sheet emerges), (3) the eruptive phase with strong acceleration of the filament, during which a large current is induced and dissipated into the current sheet, and energy is injected into the postflare loops, (4) the post-flare phase (filament acceleration declines and the current sheet vanishes).

In the view of Shibata (based on Yokohoh discoveries) the erupting features correspond to the plasmoid, similar to the LDE (long duration events) flares associated with the $H\alpha$ filament eruption. A very faint SXR intensity of the erupting features implies that the electron density is not high in there, from what

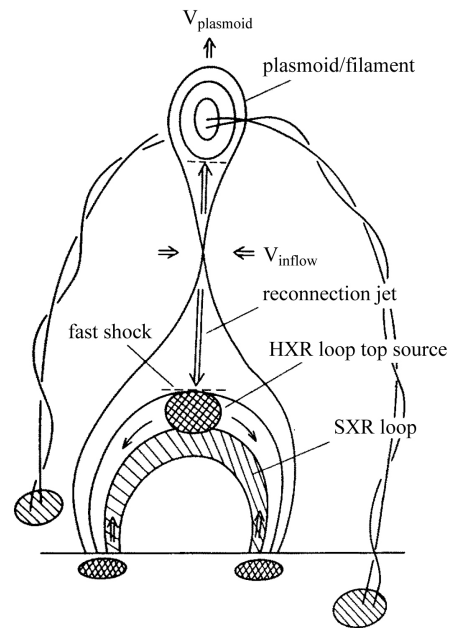


Fig. 13. A reconnection-plasmoid ejection model for compact loop flares. Note that plasmas confined by a closed field (in two-dimensions) or by a helically twisted flux tube (in three-dimension) are called *plasmoids*, as often used in magnetospheric community. In the classical picture of the two ribbon flares, the cool ($\approx 10^4$ K) plasmas associated with the twisted flux tube is the filament or prominence. Hot ($> 10^6$ K) plasma ejections are expected to be associated with the twisted tube or expanding loop high above the reconnected (SXR) loop. The cross-hatched region at the footpoints of the SXR loop shows the bright HXR/SXR double sources. The hatched region at the footpoints of the expanding (helical) loop penetrating the plasmoid shows predicted HXR/SXR distant sources. The same structure is visible on the RHESSI sequence on Fig. 14.

the total kinetic energy of the eruptions is an order of magnitude smaller than the total released energy during the impulsive phase, estimated from the HXR data. It is concluded that the eruptions are not the energy source of the flares, but simply triggered the flares. It is suggested, that the energy is stored in the magnetic field around the current sheet and the plasmoid. On the basis of these considerations, the unified model of LDE and impulsive flares is the following. The model begins with a hypothesis that the impulsive phase corresponds to the initial phase of plasmoid ejection. From observations, $V_{plasmoid} \approx 50 - 400$ km/s. Ejection of plasmoid induces a strong inflow into the X-point, which drives the fast reconnection. The velocity of inflow is estimated to be $V_{inflow} \approx V_{plasmoid}$, from the mass conservation law assuming that plasma density does not change much during the process. The magnetic reconnection theory predicts two oppositely directed high speed jets from the reconnection point at Alfvén speed, $V_{jet} \approx V_A \approx 3000(B/100G)(n_e/10^{10}cm^{-3})^{-1/2}$ km/s. The downward jet collides with the top of the SXR loop, producing MHD fast shock, supershot plasmas and/or high energy electrons at the loop top, as observed in the HXR images. Similar process was expected for the upward direction, but they found a SXR bright point during the impulsive phase somewhat far from the SXR loop. This bright point seems to be located at the footpoint of the erupting loop. The magnetic energy stored around the current sheet and the plasmoid is suddenly released through reconnection into kinetic and thermal/nonthermal energies after the plasmoid is

ejected. The magnetic energy release rate at the current sheet is estimated to be comparable with the energy release rate during the impulsive phase ($4 - 100 \times 10^{27}$ erg/s estimated from HXR data). The reason why the HXR loop top source is not bright in SXR is that the evaporation flow has not yet reached the colliding point and hence the electron density (and so the emission measure) is low. The key parameter discriminating impulse flares and LDE flares (or impulsive phase and gradual phase) is V_{inflow} . If V_{inflow} is large, the reconnection is fast, so that the reconnected field lines accumulate very fast and hence the MHD fast shock (i.e. the HXR loop top source) is created well above the SXR loop which is filled with evaporated plasmas. If V_{inflow} is small, the reconnection is slow and hence the fast shock is produced at the SXR loop. In that case, the density of the socked region is high because of evaporation, and so the temperature behind the fast sock agrees with the temperature found at the loop top in gradual phase of impulsive flares and LDE flares. The bright knots at the tops of SXR loops also seem to be explained by this model. See the article for details (and numbers).

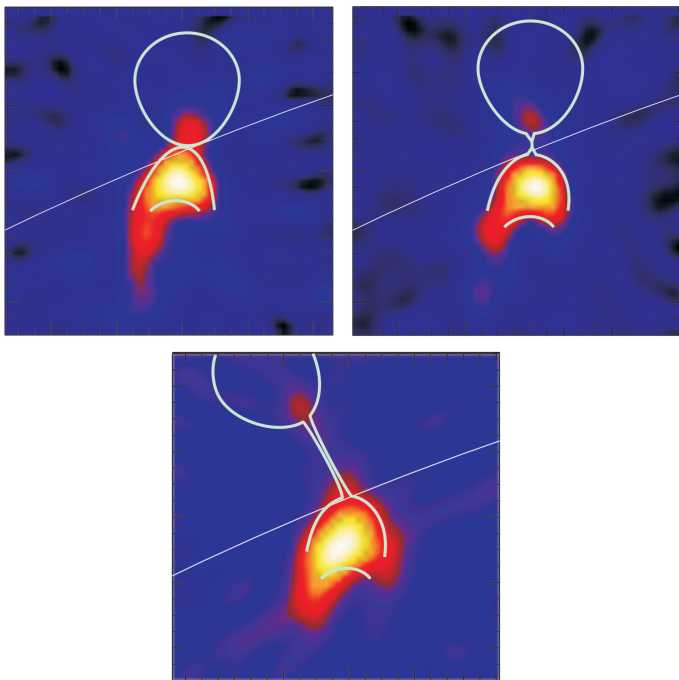


Fig. 14. False-color images of Solar X-rays detected by RHESSI (Reuven Ramaty High Energy Solar Spectroscopic Imager). It first observed an X-ray arch with a hot blob at its top (top row, left image). The blob may have been associated with a magnetic X-point, where oppositely directed magnetic fields come into contact and very slow reconnection can occur. The blob separated from the arch when the most energetic X-rays from the flare rapidly brightened (top row, right). This separation was probably associated with the collapse of the magnetic X-point to a thin region of rapid magnetic reconnection. Two minutes later, the X-ray blob sped away from the Sun (bottom). This was associated with the ejection of the upper magnetic structure from the Sun and the upward elongation of the reconnection layer. Credit: NASA

3.3. Coronal Mass Ejections

Current knowledge of CME kinematics indicates that the CME starts with an initial pre-acceleration phase characterised by a slow rising motion, followed by a period of rapid acceleration away from the Sun until a near-constant velocity is reached.

Some “balloon” CMEs (usually the very slowest ones) lack this three-stage evolution, instead accelerating slowly and continuously throughout their flight. Even for CMEs with a well-defined acceleration stage, the pre-acceleration stage is often absent (or perhaps unobservable).

On one of the last days of the semester, Carla Jacobs gave a very good and detailed PhD defence in this topic (*Magnetohydrodynamic modelling of the Solar wind and coronal mass ejections*), showing the current state of this research field with the presentation of her numerical modeling and the comparison of the real life data and the results from the model. It was clear, that the three-part structure of the CMEs is “easy” to reproduce, and the trends in the curves of different parameters of the Solar wind changing over time are now fitting the real curves well, but there are several details still beyond the range of the model.

In the following I will just mention the two top cited articles from the ADS (saw them also in the PhD defence and in the lecture) here. In the article of Antiochos, DeVore, & Klimchuk (1999) they proposed a new model for the initiation of a Solar coronal mass ejection (CME). The model agrees with two properties of CMEs and eruptive flares that have proved to be very difficult to explain with previous models: (1) very low-lying magnetic field lines, down to the photospheric neutral line, can open toward infinity during an eruption; and (2) the eruption is driven solely by magnetic free energy stored in a closed, sheared arcade. Consequently, the magnetic energy of the closed state is well above that of the posteruption open state. The key new feature of our model is that CMEs occur in multipolar topologies in which reconnection between a sheared arcade and neighbouring flux systems triggers the eruption. In this “magnetic breakout” model, reconnection removes the unshaped field above the low-lying, sheared core flux near the neutral line, thereby allowing this core flux to burst open. They present numerical simulations that demonstrate that their model can account for the energy requirements for CMEs. They also discuss the implication of the model for CME/flare prediction.

A different mechanism was proposed by Amari, Luciani, Mikic, & Linker (2000). They present a new approach to the theory of large-scale Solar eruptive phenomena such as coronal mass ejections and two-ribbon flares, in which twisted flux tubes play a crucial role. They show that it is possible to create a highly nonlinear three-dimensional force-free configuration consisting of a twisted magnetic flux rope representing the magnetic structure of a prominence (surrounded by an overlaying, almost potential, arcade) and exhibiting an S-shaped structure (Fig. 15), as observed in soft X-ray sigmoid structures. They also show that this magnetic configuration cannot stay in equilibrium and that a considerable amount of magnetic energy is released during its disruption. Unlike most previous models, the amount of magnetic energy stored in the configuration prior to its disruption is so large that it may become comparable to the energy of the open field.

4. Connection between different phenomena

The previously described phenomena are tightly connected, as I already mentioned it several times above. For example, many of the quiescent prominences disappear abruptly, expelled through the corona into interplanetary space embedded within a coronal mass ejection. CMEs and flares were at first thought to be directly connected, with the flare driving the CME. However, only 60% of flares (M-class and stronger) are associated with CMEs (Andrews 2003). Similarly, many CMEs are not associated with

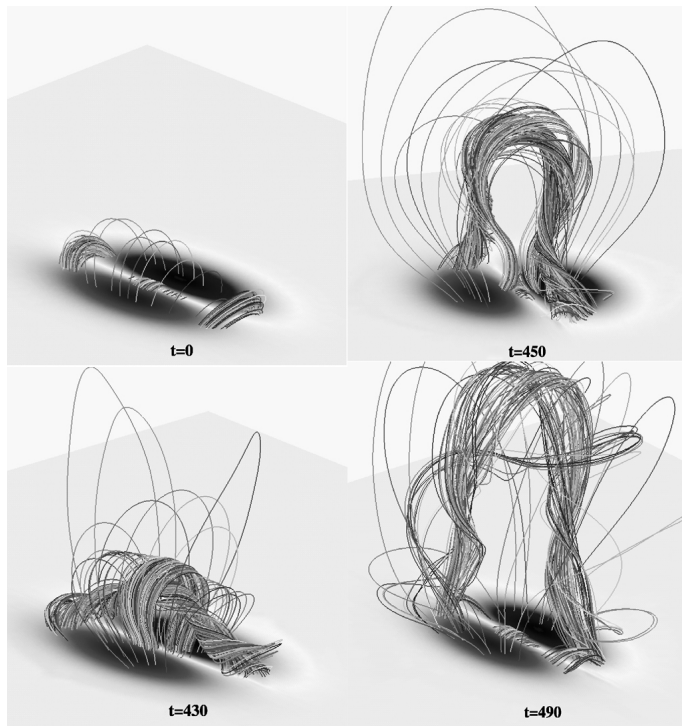


Fig. 15. Selected field line of the configuration at two steps of the MHD evolution in units of τ_A Alfvén time: (top left) $t = 0$, and (bottom left) $t = 430$ when a twisted flux rope has been created, and the evolution of the configuration at two steps during a relaxation phase at (top right) $t = 450$ and (bottom right) $t = 490$. No neighbouring equilibria exist, and the configuration experiences a major disruption.

flares. It is now thought that CMEs and associated flares are caused by a common event (the CME peak acceleration and the flare peak radiation often coincide).

2/3 of CMEs are related to eruptive prominences, but only 10% of all eruptive prominences (the biggest) are related to CMEs. CMEs are not caused by the eruptions! They precede the DB or flare, and may occur without DB or flare. The cause is a global destabilization of the magnetic structure of the corona, causing the arcade to open up and releasing the filament.

In general, all of these events (including the CMEs) are thought to be the result of a large-scale restructuring of the magnetic field. Sometimes it is possible to follow the whole process of eruption beginning from filament activation and up to the CME formation (Filippov et al. 2005).

Finally, here is a short list of articles I found about this topic: Gilbert et al. (2000) about active and eruptive prominences and their relationship to coronal mass ejections, Koutchmy et al. (2004) about the CME on 11 August 1999 observed by instruments on board LASCO and SOHO – they made a connection between the CME and a surface event, Plunkett et al. (2000) about simultaneous SOHO and ground-based observations of a large eruptive prominence and coronal mass ejection, etc.

5. Conclusion

In this task, I gave a detailed report about the most important activity phenomena of the Sun above the photosphere – prominences, flares and coronal mass ejections – starting with a brief introduction about space weather and the Solar cycle. I included the basic observational characteristics, detailed classifi-

cation schemes, short history and the list and some recent results of special instruments on ground and from space.

For the section about the modeling I made a literature study and used the most highly cited articles to present the basic topological models and some of the recent simulations. From the number of different models it is clear, that there are still a lot of questions remaining for the new generations to answer, and there is also a need for better and even more detailed observations. The main reason why we need this kind of research is that making better space weather predictions is crucial for the stability of our strongly technology dependent society.

References

- Amari, T., Luciani, J. F., Mikic, Z., & Linker, J. 2000, *ApJ*, 529, L49
 Andrews, M. D. 2003, *Sol. Phys.*, 218, 261
 Antiochos, S. K., DeVore, C. R., & Klimchuk, J. A. 1999, *ApJ*, 510, 485
 Anzer, U. & Heinzel, P. 2005, *ApJ*, 622, 714
 Athay, R. G., Quercfeld, C. W., Smartt, R. N., Degl'Innocenti, E. L., & Bommier, V. 1983, *Sol. Phys.*, 89, 3
 Bommier, V., Degl'Innocenti, E. L., Leroy, J.-L., & Sahal-Brechot, S. 1994, *Sol. Phys.*, 154, 231
 Choe, G. S. & Lee, L. C. 1992, *Sol. Phys.*, 138, 291
 Cox, D. P. & Tucker, W. H. 1969, *ApJ*, 157, 1157
 Crifo, F., Picat, J. P., & Cailloux, M. 1983, *Sol. Phys.*, 83, 143
 Field, G. B. 1965, *ApJ*, 142, 531
 Filippov, B. P., Den, O. G., & Zagnetko, A. M. 2005, in *IAU Symposium*, Vol. 226, *Coronal and Stellar Mass Ejections*, ed. K. Dere, J. Wang, & Y. Yan, 464–469
 Galsgaard, K. & Longbottom, A. W. 1999, *ApJ*, 510, 444
 Gilbert, H. R., Holzer, T. E., Burckpile, J. T., & Hundhausen, A. J. 2000, *ApJ*, 537, 503
 Hale, G. E., Ellerman, F., Nicholson, S. B., & Joy, A. H. 1919, *ApJ*, 49, 153
 Hale, G. E. & Nicholson, S. B. 1925, *ApJ*, 62, 270
 Heinzel, P. 2007, in *Astronomical Society of the Pacific Conference Series*, Vol. 368, *The Physics of Chromospheric Plasmas*, ed. P. Heinzel, I. Dorotovič, & R. J. Rutten, 271–+
 Illing, R. M. E. & Hundhausen, A. J. 1986, *J. Geophys. Res.*, 91, 10951
 Kippenhahn, R. & Schlüter, A. 1957, *Zeitschrift für Astrophysik*, 43, 36
 Koutchmy, S., Baudin, F., Bocchialini, K., et al. 2004, *A&A*, 420, 709
 Kuperus, M. & Raadu, M. A. 1974, *A&A*, 31, 189
 Leroy, J. L., Bommier, V., & Sahal-Brechot, S. 1983, *Sol. Phys.*, 83, 135
 Low, B. C. 1994, *Physics of Plasmas*, 1, 1684
 Low, B. C. & Petrie, G. J. D. 2005, *ApJ*, 626, 551
 MacQueen, R. M., Eddy, J. A., Gosling, J. T., et al. 1974, *ApJ*, 187, L85+
 Malherbe, J. M. & Priest, E. R. 1983, *A&A*, 123, 80
 Martens, P. C. H. & Kuin, N. P. M. 1989, *Sol. Phys.*, 122, 263
 Maunder, E. W. 1922, *MNRAS*, 82, 534
 Pikel'Ner, S. B. 1971, *Sol. Phys.*, 17, 44
 Plunkett, S. P., Vourlidas, A., Šimberová, S., et al. 2000, *Sol. Phys.*, 194, 371
 Pneuman, G. W. 1983, *Sol. Phys.*, 88, 219
 Priest, E. R., Hood, A. W., & Anzer, U. 1989, *ApJ*, 344, 1010
 Rutten, R. J. 1999, in *Astronomical Society of the Pacific Conference Series*, Vol. 184, *Third Advances in Solar Physics Euroconference: Magnetic Fields and Oscillations*, ed. B. Schmieder, A. Hofmann, & J. Staude, 181–200
 Shibata, K. 1996, *Advances in Space Research*, 17, 9
 Shibata, K., Masuda, S., Shimojo, M., et al. 1995, *ApJ*, 451, L83+
 Sime, D. G., MacQueen, R. M., & Hundhausen, A. J. 1984, *J. Geophys. Res.*, 89, 2113
 Zirin, H. & Severny, A. 1961, *The Observatory*, 81, 155
 Zirker, J. B. & Koutchmy, S. 1990, *Sol. Phys.*, 127, 109
 Zirker, J. B. & Koutchmy, S. 1991, *Sol. Phys.*, 131, 107